

Some inflationary models under the light of Planck 2018 results

Daniel Pozo¹, Jordan Zambrano¹, Ismael Villegas¹, Rafael Hernández–Jiménez², and Clara Rojas¹

¹ *Yachay Tech University, School of Physical Sciences and Nanotechnology, Hda. San José s/n y Proyecto Yachay, 100119, Urcuquí, Ecuador*

² *Departamento de Física, Centro Universitario de Ciencias Exactas e Ingeniería, Universidad de Guadalajara
Av. Revolución 1500, Colonia Olímpica C.P. 44430, Guadalajara, Jalisco, México*

Abstract

In this work we study four well-known inflationary scenarios that are reported by the most recent Planck observations: Natural inflation, Hilltop quartic inflation, Starobinsky inflationary model, and Large field power-law potentials $V(\phi) \sim \phi^p$, considering $p = 2/3, 4/3$. The analysis is done using both the slow-roll approximation and the numerical solution to the background and perturbation equations. We show that the numerical solution improved the precision of these models with respect to the contour plot r vs. n_s , having a lower r in each model compared to the value calculated from the slow-roll approximation.

Keywords: Cosmological Perturbations; Inflation; Inflationary Models; Slow-roll Approximation.

1. Introduction

Inflation is an epoch of accelerated expansion of the Universe introduced in the 1980's to solve the shortcomings of the Big Bang [1, 2, 3, 4, 5]. The most important of these issues are: the horizon problem, the flatness problem,

Email address: crojas@yachaytech.edu.ec (Daniel Pozo¹, Jordan Zambrano¹, Ismael Villegas¹, Rafael Hernández–Jiménez², and Clara Rojas¹)

and the unwanted magnetic monopoles. The first one related to the fact of the limit of the speed of light and treats with the causality of homogeneous distribution of heterogeneity of the temperature seen in the CMB image, the second one treats a fine-tuning problem about the curvature of the space at very few moments from the big bang [6], and the last one arises from the fact that the expected density of magnetic monopoles from calculations of Grand Unified Theory (GTU) does not match with the never recorded measurement of such relics [7, 8].

These fine tuning inconveniences not only were precursors of doubts and incompleteness regarding the hot big bang theory, but also create some philosophical inquiries about how these so unlike circumstances happened to give place to our universe. In that way, inflation plays a crucial role not only in giving an explanation for these conditions but making them into consequences.

Moreover, inflation also presents two relevant features, provided its quantum fluctuations. They yield a spectrum of scalar perturbations and a primordial background of gravitational waves. Therefore, we have a quantum perturbation theory of the isotropic and homogeneous Friedmann–Lemaître–Robertson–Walker (FLRW) universe [9, 10]. By studying these scalar and tensor perturbations, we can model and contrast them with observational Planck data [11]. Remarkably, these quantum fluctuations could be the seeds of the initial conditions observed throughout the large-scale structure of the universe [12]. Therefore, understanding their spectrum allows us to select models that produce the best fit with respect to observational data. Recently, a numerical method based in a Monte Carlo approach has been proposed in the literature to give theoretical predictions of the observables such as the amplitude of the scalar and tensor perturbations and the spectral index for scalar perturbations [13].

Throughout the years, several single field inflation scenarios have been proposed in the literature [14, 15, 16], but only a few are supported by the Planck 2018 results [11]. All are represented by the potential of the inflaton (ϕ) $V = V(\phi)$. The upshots of such survey allow us to discern among them; in fact, there is evidence that Planck’s outcome favors concave inflationary potentials, as we can observe in Fig. 1, where it is shown the primordial tilt n_s and tensor-to-scalar tensor r , as well as their correspondence levels of confidence contour plots, taken from Planck 2018 data [11].

In this work, we study four inflationary models already analyzed by Planck 2018 [11]: Natural inflation [17, 18]; Hilltop inflation [19]; Starobin-

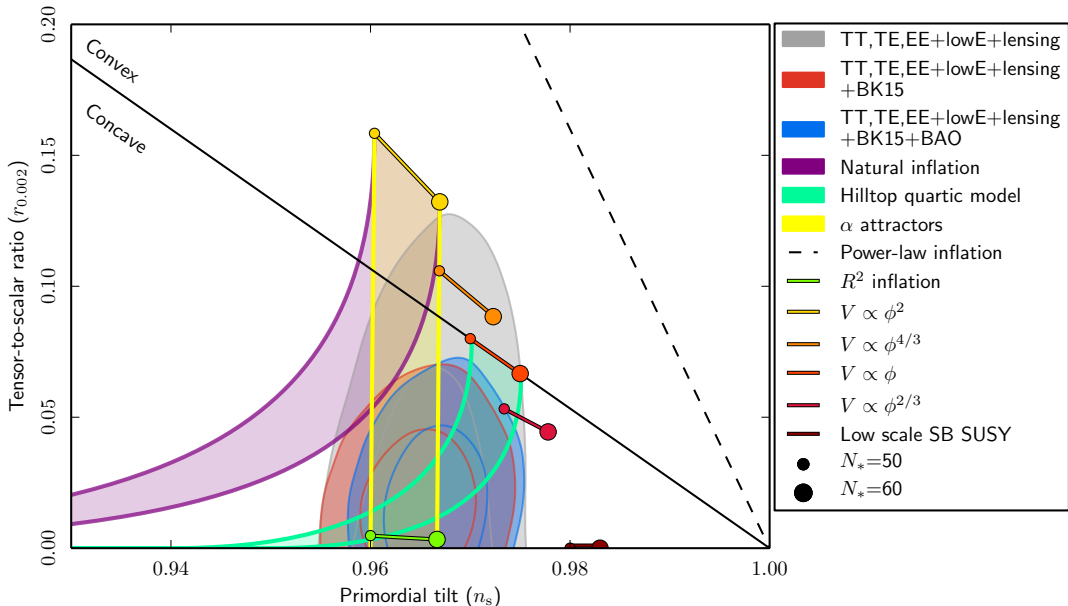


Figure 1: Contour (n_s, r) showing the Planck 2018 data and the slow-roll calculations for some inflationary models. Figure taken from Ref. [11].

sky inflationary model [20]; and Large-Field inflation [21]. Note that two of these scenarios are well inside the Planck contours: Hilltop quartic and Starobinsky (or R^2). And here $n_s = 0.9649 \pm 0.0044$ and small values for r .

According to background dynamics, accelerated expansion occurs when the potential energy of the field, $V(\phi)$, dominates over its kinetic counterpart, $\dot{\phi}^2/2$. This approach is called slow-roll inflation. We proceed using this method to obtain the initial and final states of the inflaton ϕ values, taking into account the cases for $N = 50$, and $N = 60$. Once we have obtained such estimates, we use them as initial conditions for our numerical implementation.

This article is structured as follows: in Section 2 we introduce the background and perturbations equations. Then in Section 3 we present the slow-roll analysis and the formulas of the observables under this approximation. In Section 4 we follow our numerical procedure to solve the aforementioned system of equations. Next, in Section 5 we show the corresponding analysis of each inflationary model considered in this project. Therefore, in Section 6 we examine and discuss our results. Finally, in Section 7 we present our conclusions of this work.

2. Equations of motion of Background and Perturbations

The equations of motion of the inflaton ϕ and the Hubble parameter H (with $M_{\text{Pl}} = 1$) are given by [22],

$$H^2 = \frac{1}{3} \left[V(\phi) + \frac{1}{2} \dot{\phi}^2 \right], \quad (1)$$

$$\ddot{\phi} + 3H\dot{\phi} = -\frac{\partial V(\phi)}{\partial \phi}, \quad (2)$$

where the dots indicate derivatives with respect to physical time t , and $\partial V(\phi)/\partial \phi$ is the derivative of the potential energy with respect to the ϕ .

Eq. (1) is the Friedmann equation in terms of the scalar field, and Eq. (2) represents the inflaton dynamics.

The scalar perturbations formulas come from a quantum perturbation theory, as well as linear fluctuations to the FLRW metric; having [12],

$$u_k'' + \left(k^2 - \frac{z_S''}{z_S} \right) u_k = 0, \quad (3)$$

where $z_S = a\phi'/\mathcal{H}$, $\mathcal{H} = a'/a$. Here, the prime indicates derivative with respect to the conformal time τ . The relation between t and τ is given by equation $dt = a d\tau$.

For tensor perturbations, one introduces the function $v_k = ah$, where h represents the amplitude of the gravitational wave. Tensor perturbations obey a second order differential equation given by [12],

$$v_k'' + \left(k^2 - \frac{a''}{a} \right) v_k = 0. \quad (4)$$

Considering the limits $k^2 \gg |z_S''/z_S|$ (short wavelength) and $k^2 \ll |z_S''/z_S|$ (long wavelength), we have the solutions of Eq. (3) present the following asymptotic behavior,

$$u_k \rightarrow \frac{e^{-ik\tau}}{\sqrt{2k}} \quad (k^2 \gg |z_S''/z_S|, -k\tau \rightarrow \infty), \quad (5)$$

$$u_k \rightarrow A_k z \quad (k^2 \ll |z_S''/z_S|, -k\tau \rightarrow 0). \quad (6)$$

And the same asymptotic conditions hold for tensor perturbations. Hereafter Eq. (5) will be used as the initial condition for the perturbations.

On the other hand, the power spectra of the scalar and tensor perturbations are given by the expressions,

$$P_S(k) = \lim_{k\tau \rightarrow 0^-} \frac{k^3}{2\pi^2} \left| \frac{u_k(\tau)}{z_S(\tau)} \right|^2, \quad (7)$$

$$P_T(k) = \lim_{k\tau \rightarrow 0^-} \frac{k^3}{2\pi^2} \left| \frac{v_k(\tau)}{a(\tau)} \right|^2, \quad (8)$$

and the scalar spectral index together with its running are defined by,

$$n_S(k) = 1 + \frac{d \ln P_S(k)}{d \ln k}, \quad (9)$$

$$\alpha_S(k) = \frac{d n_S(k)}{d \ln k}. \quad (10)$$

In addition, the tensor-to-scalar ratio r is defined as,

$$r = 8 \frac{P_T(k)}{P_S(k)}. \quad (11)$$

Notice also that for single field models, the tensor-to-scalar ratio r can be related to the tilt of the tensor spectrum of perturbations, this is the tensor spectral index n_T , by the consistency equation [23],

$$n_T(k) = -\frac{r}{8}. \quad (12)$$

3. Slow-roll analysis

The slow-roll approximation is considered the standard technique used in inflation. This approach considers that $V(\phi) \gg \dot{\phi}$; additionally by differentiating this suggests the further condition $|\dot{\phi}| \ll |V_\phi|$; however, note that derivatives of approximations need not themselves be valid approximations, and so this is an additional condition. Then we also neglect the $\ddot{\phi}$ term from Eq. (2). Thus, the background equations of motion (1) and (2) are simplified in the following way,

$$H^2 \simeq \frac{1}{3}V(\phi), \quad (13)$$

$$3H\dot{\phi} \simeq -\frac{\partial V(\phi)}{\partial \phi}. \quad (14)$$

An inflationary model is sometimes parameterized by expanding the potential in a Taylor series, i.e., in higher and higher derivatives of $V(\phi)$. The first two so called slow-roll parameters,

$$\epsilon = \frac{1}{2} \left(\frac{V'}{V} \right)^2, \quad (15)$$

$$\eta = \frac{V''}{V}, \quad (16)$$

where the prime indicates derivative respect to ϕ . The first one measures the slope of the potential, and the second one the curvature. The amount by which the universe inflates is measured as the number of e-foldings, giving by,

$$N \simeq \int_{\phi_{\text{end}}}^{\phi} \frac{V}{V'} d\phi, \quad (17)$$

where ϕ_{end} is the value of the scalar field at the end of inflation.

Moreover, the scalar power spectrum $P_S(k)$ and the tensor power spectrum $P_T(k)$ from the slow-roll approximation are given by the expressions [24],

$$P_S(k) \simeq \frac{1}{12\pi^2} \frac{V^3}{V'^2} \left[1 - \left(2C + \frac{1}{6} \right) \epsilon + \left(C - \frac{1}{3} \right) \eta \right], \quad (18)$$

$$P_T(k) \simeq [1 - (C + 1) \epsilon_H]^2 \left(\frac{H}{2\pi} \right)^2 \Big|_{k=aH}, \quad (19)$$

where $C = -2 + \ln 2 + b \simeq -0.729637$, here b is the Euler-Mascheroni constant, and

$$\epsilon_H = \epsilon \left(1 - \frac{2}{3} \epsilon + \frac{1}{3} \eta \right). \quad (20)$$

Furthermore, the scalar spectral index $n_S(k)$ and the tensor-to-scalar ratio r from the slow-roll approximation are given, in terms of the slow-roll parameters, by [22],

$$n_S \simeq 1 - 6\epsilon + 2\eta, \quad (21)$$

$$r \simeq 16\epsilon. \quad (22)$$

Expressions (18), (19), (21), and (22) must be to evaluate at horizon crossing $k = aH$, and explicitly depend on the inflaton value at that instance ϕ_* , which depends on time t_* . Thus, for each k one obtains a value of $\phi_*(t_*)$ that is then substituted into Eqs. (18), (19), (21), and (22).

Finally, from an additional approximation of the scalar power-spectrum $P_S(k)$, that is [22],

$$\delta_R = \frac{1}{24\pi^2} \frac{V(\phi)}{\epsilon(\phi)}, \quad (23)$$

we calculate the free parameter M , that characterizes each inflationary model, by fixing $\delta_R \sim 2.1 \times 10^{-9}$ (COBE normalization), at the pivot scale $k_* = 0.05 \text{ Mpc}^{-1}$ [25].

4. Numerical analysis

In this section, we present our numerical implementation. To solve the perturbation equations numerically, first we have to solved the equations of motion Eq. (1) and Eq. (2) numerically with respect to physical time t taking as initial conditions the slow-roll solutions. Hence, the scale factor $a_{\text{sr}}(t)$, the scalar field $\phi_{\text{sr}}(t)$, and the derivative with respect to the physical time of the scalar field $\dot{\phi}_{\text{sr}}$ are obtained into the slow-roll approximation, and evaluated at $t = 0$. The integration is made from $t_{\text{ini}} = 0$ until the end of inflation t_{end} , whic is calculated in each case. From the four model studied only three have analytical solution for the slow-roll approximation: the Natural, Starobinsky and large field inflationary models. In the case of the Hilltop potential we have to solve numerically the slow-roll equations Eqs. (13) and (14), in this case the integration is also made from $t_{\text{ini}} = 0$ until the end of inflation t_{end} .

On the other hand, the equations of the linear fluctuations are τ dependent, so we proceed to rewrite them in terms of the variable t . Therefore, these equations are,

$$\ddot{u}_k + \frac{\dot{a}}{a} \dot{u}_k + \frac{1}{a^2} \left[k^2 - \frac{(\dot{a}\dot{z}_S + a\ddot{z}_S)a}{z_S} \right] u_k = 0, \quad (24)$$

$$\ddot{v}_k + \frac{\dot{a}}{a} \dot{v}_k + \frac{1}{a^2} [k^2 - (\dot{a}^2 + a\ddot{a})] v_k = 0, \quad (25)$$

where z_S , \dot{z}_S , and \ddot{z}_S are given in terms of a , ϕ , and their time t derivatives,

$$z_S = \frac{a^2 \dot{\phi}}{\dot{a}}, \quad (26)$$

$$\dot{z}_S = a \dot{\phi} \left(2 - \frac{a\ddot{a}}{\dot{a}^2} \right) + \frac{a^2 \ddot{\phi}}{\dot{a}}, \quad (27)$$

$$\begin{aligned} \ddot{z}_S = & 2\dot{a}\dot{\phi} + \frac{2a^2\ddot{a}^2\dot{\phi}}{\dot{a}^3} + 4a\ddot{\phi} - \frac{a^2(2\ddot{a}\ddot{\phi} + \ddot{a}\dot{\phi})}{\dot{a}^2} \\ & + \frac{a(-2\ddot{a}\dot{\phi} + a\ddot{\phi})}{\dot{a}}. \end{aligned} \quad (28)$$

The equations for the scalar and tensor perturbations (24) and (25), respectively, are then numerically integrated. Note that u_k and v_k are complex functions, then two differential equations are solved for each of them, both real and imaginary parts. Integration is performed in two instances. The first part is done in the limit when $k^2 \gg (\dot{a}z_S + az_S')/z_S$, and $k^2 \gg \dot{a}^2 + a\ddot{a}$ for scalar and tensor perturbations, respectively, so the differential equation to solved are the following,

$$\ddot{u}_k + \frac{\dot{a}}{a}\dot{u}_k + \frac{k^2}{a^2}u_k = 0, \quad (29)$$

$$\ddot{v}_k + \frac{\dot{a}}{a}\dot{v}_k + \frac{k^2}{a^2}v_k = 0, \quad (30)$$

the integration is done from $t_{\text{ini}} = 0.001 h_c(k)$ until $t_{\text{end}} = 0.05 h_c(k)$, where $h_c(k)$ is the horizon defined by the time where the mode freezes $k = aH$. In this stage, we have used as initial condition Eq. (5) but written in terms of t , that is $\tau \simeq -1/[a(t)H]$ since H is nearly constant inside the horizon ¹, then u_k and v_k exhibits an oscillatory behavior.

Then, we use the final stage of this solution as an initial condition to solve the complete set of Eqs. (24) and (25) from $k = 0.0001 \text{ Mpc}^{-1}$ to

¹In particular, during inflation,

$$\tau = \int_0^a \frac{da}{Ha^2} \simeq \frac{1}{H} \int_0^a \frac{da}{a^2} \simeq -\frac{1}{aH}.$$

$k = 10 \text{ Mpc}^{-1}$, and the integration is done from $t_{\text{ini}} = 0.05 h_c(k)$ until $t_{\text{end}} = 3 h_c(k)$, when the perturbations are already frozen. Finally, from Eqs. (7) and (8) we calculated the scalar and tensor power spectra.

Also, in order to find the scalar spectral index $n_S(k)$ we implement the fit of the scalar power spectrum $P_S(k)$ with a power-law form [26, 27, 28], that is,

$$P_S(k) = A_S \left(\frac{k}{k_*} \right)^{n_S - 1 + \frac{1}{2} \alpha_S \ln\left(\frac{k}{k_*}\right)}, \quad (31)$$

so that $P_S(k)$ becomes scale dependent. Here, A_S is the amplitude of the scalar power spectrum, and α_S is the running of the scalar spectral index. Equation (31) is evaluated at a given pivot scale $k_* = 0.002 \text{ Mpc}^{-1}$, and $k_* = 0.05 \text{ Mpc}^{-1}$.

Then, to find the tensor-to-scalar ratio r we also utilize the fit of the tensor power spectrum $P_T(k)$ with a power-law form [7, 29, 27],

$$P_T(k) = A_T \left(\frac{k}{k_*} \right)^{n_T + \frac{1}{2} \alpha_T \ln\left(\frac{k}{k_*}\right)}, \quad (32)$$

where A_T is the amplitude of the tensor power spectrum, and α_T is the running of the tensor spectral index. Equation (32) is evaluated at a given pivot scale $k_* = 0.002 \text{ Mpc}^{-1}$.

The relation between the scalar power spectrum $P_S(k)$ and the amplitude of the scalar power spectrum A_S , without considering the running of the scalar spectral index α_S , is given by [11],

$$\ln P_S(k) = \ln A_S + (n_S - 1) \ln \left(\frac{k}{k_*} \right), \quad (33)$$

here Planck takes as pivot scale $k_* = 0.05 \text{ Mpc}^{-1}$ [11]. Finally, we evaluate the scalar power spectrum $P_S(k)$ at $k = 0.05 \text{ Mpc}^{-1}$, therefore $P_S(k)$ becomes equal to A_S .

5. Models of inflation

5.1. Natural Inflation

Natural inflation was introduced in 1990 [17, 18] as a proposal to generate an inflationary epoch. Although this model was consistent with Planck 2015 data [30], currently it is disfavored by the newest version Planck 2018 plus

the BK15 data [11, 31]. However, considering a prolonged reheating period, natural inflation returns to the 95% of confidence levels of Planck observations [32]. Furthermore, in the warm inflation scenario, natural inflation is consistent with the constraints of n_s and r from Planck 2018 data [33].

The natural inflation potential is given by [34, 11, 15],

$$V(\phi) = M^4 \left[1 + \cos \left(\frac{\phi}{f} \right) \right], \quad (34)$$

where M is a free parameter to be determined by the normalization of the scalar power spectrum $P_S(k)$, and $0.3 < \log_{10} f < 2.5$ [11]. The behavior of the potential is shown in Fig. 2. Inflation occurs from left to right, so the field ϕ slowly rolls near a maximum of the potential to its minimum.

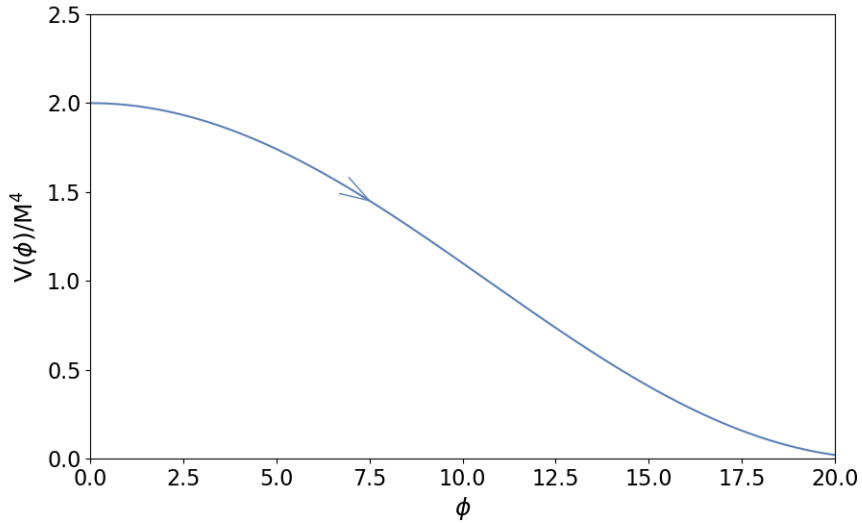


Figure 2: Inflationary potential for Natural Inflation using $f = 6.8$.

From Eqs. (15) and (16) we calculate analytically the slow-roll parameters, yielding,

$$\epsilon = \frac{1}{2f^2} \frac{\sin^2\left(\frac{\phi}{f}\right)}{\left[1 + \cos\left(\frac{\phi}{f}\right)\right]^2}, \quad (35)$$

$$\eta = -\frac{1}{f^2} \frac{\cos\left(\frac{\phi}{f}\right)}{\left[1 + \cos\left(\frac{\phi}{f}\right)\right]}. \quad (36)$$

When $\epsilon = 1$ inflation ends, so the value for the scalar field at the end of inflation is given by,

$$\phi_{\text{end}} = f \arccos\left(\frac{1 - 2f^2}{1 + 2f^2}\right). \quad (37)$$

The number of e-foldings is calculated from equation (17), that is,

$$N \simeq f^2 \ln \left[\frac{1 - \cos(\phi_{\text{end}}/f)}{1 + \cos(\phi_{\text{end}}/f)} \right]. \quad (38)$$

Fixing the number of e-foldings between 50 – 60 e-folds we can obtain ϕ_{ini} as,

$$\phi_{\text{ini}} = f \arccos \left\{ 1 - \left[1 - \cos\left(\frac{\phi_{\text{end}}}{f}\right) \right] e^{-N/f^2} \right\}. \quad (39)$$

Replacing ϕ_{end} [from Eq. (37)] in Eq. (39) we obtain,

$$\phi_{\text{ini}} = f \arccos \left(1 - \frac{4f^2}{1 + 2f^2} e^{-N/f^2} \right). \quad (40)$$

Then, using the slow-roll approximations, Eqs. (13) and (14) the scale factor $a_{\text{sr}}(t)$ and the scalar field $\phi_{\text{sr}}(t)$ become,

$$\begin{aligned}
a_{\text{sr}}(t) \simeq & \exp \left\{ -2f^2 \ln \left\{ \cosh \left[\operatorname{arctanh} \left(\frac{\sqrt{1 + \cos(\phi_{\text{ini}}/f)}}{\sqrt{2}} \right) - \frac{M^2}{\sqrt{6}f^2} t \right] \right\} \right. \\
& \left. - \ln \left\{ \cosh \left[\operatorname{arctanh} \left(\frac{\sqrt{1 + \cos(\phi_{\text{ini}}/f)}}{\sqrt{2}} \right) \right] \right\} \right\}, \tag{41}
\end{aligned}$$

$$\phi_{\text{sr}}(t) \simeq f \arccos \left\{ 2 \tanh \left[\operatorname{arctanh} \left(\frac{\sqrt{1 + \cos(\phi_{\text{ini}}/f)}}{\sqrt{2}} \right) - \frac{M^2}{\sqrt{6}f^2} t \right]^2 - 1 \right\}, \tag{42}$$

here M is computed from Eq. (23), yielding,

$$M^4 = \frac{12\delta_R\pi^2 \sin^2\left(\frac{\phi_*}{f}\right)}{f^2 \left[1 + \cos\left(\frac{\phi_*}{f}\right)\right]^3}, \tag{43}$$

where ϕ_* is calculated at the horizon crossing $k = 0.05 \text{ Mpc}^{-1}$.

To solve the equation of motion numerically we integrated Eqs. (1) and (2), using as initial condition the derivative of Eq. (42) evaluated at $t = 0$, $\dot{\phi}_{\text{sr}}(0)$. The integration was done since $t_{\text{ini}} = 0$ until t_{end} . The initial condition for $\dot{\phi}_{\text{sr}}(0)$ is given by,

$$\dot{\phi}_{\text{sr}}(0) = -\frac{M^2 \left[-1 + \cos\left(\frac{\phi_{\text{ini}}}{f}\right)\right] \sqrt{1 + \cos\left(\frac{\phi_{\text{ini}}}{f}\right)}}{\sqrt{3}f \sin\left(\frac{\phi_{\text{ini}}}{f}\right)}. \tag{44}$$

In table 1 we show the value of t_{end} for each value of f that we use in our contour plots for the Natural inflation model $N = 50$, and $N = 60$.

N	f	$t_{\text{end}} \times 10^6 [\text{M}_{\text{Pl}}^{-1}]$
50	4	3.34115
	5	2.61706
	6	2.34349
	7	2.21186
	9	2.09330
	12	2.02757
	20	1.98117
	100	1.95885
60	4	5.37998
	5	3.87416
	6	3.34232
	7	3.09656
	9	2.88293
	12	2.76873
	20	2.69075
	100	2.65349

Table 1: Value of the time at the end of inflation t_{end} for each value of f in the Natural inflation scenario.

The scalar power spectrum $P_{\text{S}}(k)$, the scalar spectral index $n_{\text{S}}(k)$, and the tensor-to-scalar ratio r are calculated from Eqs. (18), (21), and (22); and they are,

$$P_{\text{S}}(k) = \frac{M^4}{144\pi^2} \left[-1 - 12C + 12f^2 + (5 + 12f^2) \cos\left(\frac{\phi_*}{f}\right) \right] \cot^2\left(\frac{\phi_*}{2f}\right), \quad (45)$$

$$n_{\text{S}}(k) = \frac{1}{f^2} \left[1 + f^2 - 2 \sec^2\left(\frac{\phi_*}{2f}\right) \right], \quad (46)$$

$$r = \frac{8}{f^2} \tan^2\left(\frac{\phi_*}{2f}\right), \quad (47)$$

where ϕ_* is calculated at $k_* = 0.05 \text{Mpc}^{-1}$, and for each value of f shown in Table 1.

5.2. Hilltop quartic inflation

Here, we consider the Hilltop quartic inflation model that fits with the Planck 2018 observational data [11, 15, 16, 34, 35, 36, 37, 38, 39, 40]. The Hilltop inflationary potential is given by [19],

$$V(\phi) = M^4 \left[1 - \left(\frac{\phi}{\mu} \right)^p \right], \quad (48)$$

where M must be fixed via the amplitude of the scalar power spectrum $P_S(k)$ given by Eq. (23), $-2 < \log_{10} \mu < 2$ [11], and $p = 4$. The form of the potential is shown in Fig. 3. Similarly as in natural inflation the field ϕ rolls down from left to right, decreasing from close to the maximum of the potential towards its minimum [41]. In fact, this kind of Hilltop model has also been considered in the context of warm inflation [42].

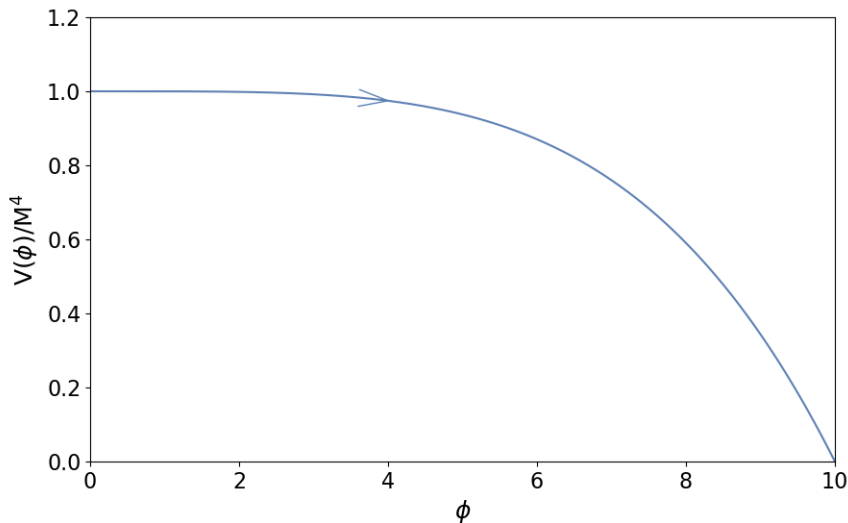


Figure 3: Inflationary potential for Hilltop quartic inflation using $\mu = 10$.

From Eqs. (15) and (16) the slow-roll parameters for this model are given by,

$$\epsilon = \frac{p^2}{2\mu^2} \frac{\left(\frac{\phi}{\mu}\right)^{2p-2}}{\left[1 - \left(\frac{\phi}{\mu}\right)^p\right]^2}, \quad (49)$$

$$\eta = -\frac{p(p-1)}{\mu^2} \frac{\left(\frac{\phi}{\mu}\right)^{p-2}}{\left[1 - \left(\frac{\phi}{\mu}\right)^p\right]}. \quad (50)$$

Inflation ends when $\epsilon = 1$, hence we calculate the expression for ϕ_{end} ,

$$\left(\frac{\phi_{\text{end}}}{\mu}\right)^p + \frac{p}{\sqrt{2}\mu} \left(\frac{\phi_{\text{end}}}{\mu}\right)^{p-1} - 1 = 0, \quad (51)$$

which must be solved numerically. Then, the number of e-foldings (Eq. (17)) is,

$$N \simeq \frac{\mu^2}{2p} \left\{ \left(\frac{\phi_{\text{ini}}}{\mu}\right)^2 - \left(\frac{\phi_{\text{end}}}{\mu}\right)^2 - \frac{2}{(2-p)} \left[\left(\frac{\phi_{\text{ini}}}{\mu}\right)^{2-p} - \left(\frac{\phi_{\text{end}}}{\mu}\right)^{2-p} \right] \right\}. \quad (52)$$

To obtain the value of ϕ_{ini} , for a given value of μ , we set $N \sim 50 - 60$. Solving the slow-roll approximation [Eqs. (13) and (14)] the scalar field $\phi_{\text{sr}}(t)$ must be computed numerically from the following expression,

$$\begin{aligned} & \frac{\phi_{\text{sr}}}{(2-p)} \left(\frac{\phi_{\text{sr}}}{\mu}\right)^{1-p} {}_2F_1 \left[-\frac{1}{2}, -1 + \frac{2}{p}, \frac{2}{p}, \left(\frac{\phi_{\text{sr}}}{\mu}\right)^p \right] \\ & - \frac{\phi_{\text{ini}}}{(2-p)} \left(\frac{\phi_{\text{ini}}}{\mu}\right)^{1-p} {}_2F_1 \left[-\frac{1}{2}, -1 + \frac{2}{p}, \frac{2}{p}, \left(\frac{\phi_{\text{ini}}}{\mu}\right)^p \right] - \frac{pM^2}{\sqrt{3}\mu} t = 0, \end{aligned} \quad (53)$$

where ϕ_{sr} depends explicitly on the physical time t , and the parameter M is fixed from Eq. (23),

$$M^4 = \frac{12\delta_R p^2 \pi^2 \left(\frac{\phi_*}{\mu}\right)^{2p}}{\phi_*^2 \left[\left(\frac{\phi_*}{\mu}\right)^p - 1 \right]^3}, \quad (54)$$

where ϕ_* is calculated at the horizon crossing $k = 0.05 \text{ Mpc}^{-1}$.

We consider the special case $p = 4$, hence Eq. (53) becomes,

$$\begin{aligned}
& - \mu \frac{\sqrt{1 - \left(\frac{\phi_{\text{sr}}}{\mu}\right)^4}}{2 \left(\frac{\phi_{\text{sr}}}{\mu}\right)^2} + \mu \arctan \left[\frac{\sqrt{1 - \left(\frac{\phi_{\text{sr}}}{\mu}\right)^4}}{1 + \left(\frac{\phi_{\text{sr}}}{\mu}\right)^2} \right] \\
& + \mu \frac{\sqrt{1 - \left(\frac{\phi_{\text{ini}}}{\mu}\right)^4}}{2 \left(\frac{\phi_{\text{ini}}}{\mu}\right)^2} - \mu \arctan \left[\frac{\sqrt{1 - \left(\frac{\phi_{\text{ini}}}{\mu}\right)^4}}{1 + \left(\frac{\phi_{\text{ini}}}{\mu}\right)^2} \right] - \frac{4M^2}{\sqrt{3}\mu} t = 0, \quad (55)
\end{aligned}$$

which is also solved numerically.

To solved the equation of motion numerically we integrated Eqs. (1) and (2), using as initial condition the numerical derivative of ϕ_{sr} evaluated at $t = 0$, which is calculated also numerically from Eqs. (13) and (14). In both cases the integration was done since $t_{\text{ini}} = 0$ until t_{end} considering $p = 4$. In table 2 we show the value of t_{end} for each value of μ that we use in our contour plots for the Hilltop inflation model for $N = 50$, and $N = 60$.

The scalar power spectrum $P_{\text{S}}(k)$, the scalar spectral index $n_{\text{S}}(k)$, and the tensor-to-scalar ratio r are obtained from Eqs. (18), (21), and (22); and they are given by,

$$\begin{aligned}
P_{\text{S}}(k) &= \frac{M^4}{144\pi^2 p^2} \left\{ -12\phi_*^2 \left[\left(\frac{\phi_*}{\mu}\right)^p - 1 \right]^2 + p \left(\frac{\phi_*}{\mu}\right)^p \left\{ 4 - 4p - 4 \left(\frac{\phi_*}{\mu}\right)^p \right. \right. \\
& \left. \left. + 5p \left(\frac{\phi_*}{\mu}\right)^p + 12C \left[\left(\frac{\phi_*}{\mu}\right)^p + p - 1 \right] \right\} \right\} \left(\frac{\phi_*}{\mu}\right)^{-2p} \left[\left(\frac{\phi_*}{\mu}\right)^p - 1 \right], \quad (56)
\end{aligned}$$

$$n_{\text{S}}(k) = 1 + p \left[2 - 2p - (2 + p) \left(\frac{\phi_*}{\mu}\right)^p \right] \frac{\left(\frac{\phi_*}{\mu}\right)^p}{\phi_*^2 \left[\left(\frac{\phi_*}{\mu}\right)^p - 1 \right]^2}, \quad (57)$$

$$r = 8p^2 \frac{\left(\frac{\phi_*}{\mu}\right)^{2p}}{\phi_*^2 \left[\left(\frac{\phi_*}{\mu}\right)^p - 1 \right]^2}, \quad (58)$$

N	μ	$t_{\text{end}} \times 10^6 [\text{M}_{\text{Pl}}^{-1}]$
50	7	8.06819
	9	5.92022
	11	4.80594
	13	4.14827
	15	3.72415
	18	3.31895
	25	2.84391
	35	2.55985
60	95	2.21469
	7	10.24704
	9	8.94586
	11	7.12657
	13	6.05813
	15	5.37257
	18	4.72167
	25	3.96524
35	3.51943	
95	2.98903	

Table 2: Value of the time at the end of inflation t_{end} for each value of μ in the Hilltop inflation scenario.

where ϕ_* is calculated at $k_* = 0.05\text{Mpc}^{-1}$, and for each value of μ shown in Table 2.

5.3. Starobinsky Inflationary Model

This scenario was introduced in 1980 by A. Starobinsky [20] and has become the best inflationary model supported by Planck data [11]. In particular, this scheme yields a small tensor-to-scalar ratio r . The form of the inflationary potential is given by [15, 43, 44, 45],

$$V(\phi) = M^4 \left(1 - e^{-\sqrt{\frac{2}{3}}\phi}\right)^2, \quad (59)$$

where M is a parameter to be fixed by the amplitude of the scalar power spectrum $P_{\text{S}}(k)$ given by Eq. (23). Inflation happens from right to left and

here the scalar field ϕ rolls slowly close to its maximum until its minimum. The behavior of the Starobinsky inflationary potential is shown in Fig. 4.

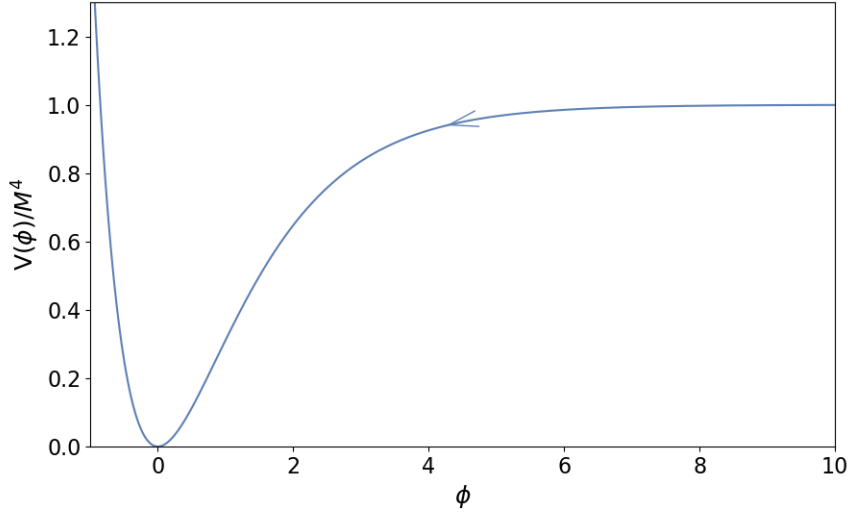


Figure 4: Inflationary potential for the Starobinsky inflationary model.

The slow-roll parameters are calculated from Eqs. (15) and (16), yielding,

$$\epsilon = \frac{4}{3} \frac{1}{\left(e^{\sqrt{\frac{2}{3}}\phi} - 1\right)^2}, \quad (60)$$

$$\eta = -\frac{4}{3} \frac{\left(e^{\sqrt{\frac{2}{3}}\phi} - 2\right)}{\left(e^{\sqrt{\frac{2}{3}}\phi} - 1\right)^2}. \quad (61)$$

Once again $\epsilon = 1$ indicates that inflation has ceased, we compute ϕ_{end} from Eq. (60), having,

$$\phi_{\text{end}} = \sqrt{\frac{3}{2}} \ln \left(\frac{2 + \sqrt{3}}{\sqrt{3}} \right). \quad (62)$$

Then, the number of e-folding is giving by,

$$N \simeq \frac{3}{4}e^{\sqrt{\frac{2}{3}}\phi_{\text{ini}}} - \frac{\sqrt{3}}{2\sqrt{2}}\phi_{\text{ini}} - \frac{3}{4}e^{\sqrt{\frac{2}{3}}\phi_{\text{end}}} + \frac{\sqrt{3}}{2\sqrt{2}}\phi_{\text{end}}. \quad (63)$$

Fixing $N \sim 50 - 60$ e-folds we compute the initial value of the scalar field ϕ_{ini} ,

$$\begin{aligned} \phi_{\text{ini}} &= -\sqrt{\frac{3}{2}} \left(1 + \frac{2}{\sqrt{3}}\right) - 2\sqrt{\frac{2}{3}}N + \sqrt{\frac{3}{2}} \ln \left(1 + \frac{2}{\sqrt{3}}\right) \\ &\quad - \frac{2}{\sqrt{3}}W_{-1} \left[-e^{-(1+\frac{2}{\sqrt{3}})-\frac{4N}{3}+\ln(1+\frac{2}{\sqrt{3}})}\right]. \end{aligned} \quad (64)$$

The slow-roll equations allow us to obtain $a_{\text{sr}}(t)$ and $\phi_{\text{sr}}(t)$, yielding,

$$a_{\text{sr}}(t) \simeq \exp \left\{ -\frac{3}{4} \left[-\frac{4}{3\sqrt{3}}M^2t + \ln \left(e^{\sqrt{\frac{2}{3}}\phi_{\text{ini}}} \right) - \ln \left(-\frac{4}{3\sqrt{3}}M^2t + e^{\left(e^{\sqrt{\frac{2}{3}}\phi_{\text{ini}}} \right)} \right) \right] \right\}, \quad (65)$$

$$\phi_{\text{sr}}(t) \simeq \sqrt{\frac{3}{2}} \ln \left(-\frac{4}{3\sqrt{3}}M^2t + e^{\sqrt{\frac{2}{3}}\phi_{\text{ini}}} \right), \quad (66)$$

where M is computed from Eq. (23) and is equal to,

$$M^4 = \frac{32\delta_R e^{2\sqrt{\frac{2}{3}}\phi_*} \pi^2}{\left(e^{2\sqrt{\frac{2}{3}}\phi_*} - 1 \right)^4}, \quad (67)$$

where ϕ_* is calculated at the horizon crossing $k = 0.05 \text{ Mpc}^{-1}$.

To solve the equation of motion numerically we integrated Eqs. (1) and (2), using as initial condition the numerical derivative of ϕ_{sr} evaluated at $t = 0$, which is calculated from Eqs. (66). The integration was done since $t_{\text{ini}} = 0$ until t_{end} . The initial condition for $\dot{\phi}_{\text{sr}}(0)$ is given by,

$$\dot{\phi}_{\text{sr}}(0) = -\frac{2}{3}\sqrt{2}M^2e^{-\sqrt{\frac{2}{3}}\phi_{\text{ini}}}. \quad (68)$$

In table 3 we show the value of t_{end} for $N = 50$, and $N = 60$.

N	$t_{\text{end}} \times 10^6 \text{ [M}_{\text{Pl}}^{-1}]$
50	6.71723
60	9.94144

Table 3: Value of the time at the end of inflation t_{end} for each value of μ in the Starobinsky inflationary model.

The scalar power spectrum $P_{\text{S}}(k)$, the spectral index $n_{\text{S}}(k)$, and the tensor-to-scalar ratio r are given by,

$$P_{\text{S}}(k) = \frac{M^4}{288\pi^2} \left[-1 - 2(7 + 6C) e^{\sqrt{\frac{2}{3}}\phi_*} + 9e^{2\sqrt{\frac{2}{3}}\phi_*} \right] e^{-2\sqrt{\frac{2}{3}}\phi_*} \left(e^{\sqrt{\frac{2}{3}}\phi_*} - 1 \right)^2, \quad (69)$$

$$n_{\text{S}}(k) = \frac{-5 - 14e^{\sqrt{\frac{2}{3}}\phi_*} + 3e^{2\sqrt{\frac{2}{3}}\phi_*}}{3 \left(e^{\sqrt{\frac{2}{3}}\phi_*} - 1 \right)^2}, \quad (70)$$

$$r = \frac{64}{3 \left(e^{\sqrt{\frac{2}{3}}\phi_*} - 1 \right)^2}, \quad (71)$$

where ϕ_* is calculated at the horizon crossing $k_* = 0.05\text{Mpc}^{-1}$.

5.4. Large field inflationary models

The large field inflationary models were first introduced by A. D. Linde in 1983 [16, 21]. These models depends on the parameter p , where the potential component is given by the expression [11, 44, 15],

$$V(\phi) = M^4 \phi^p, \quad (72)$$

here M is fixed with respect to the amplitude of the scalar power spectrum $P_{\text{S}}(k)$ given by Eq. (23). Models with $p > 2$ are already ruled out from observations; however, instances with $p = 1$ [46] and $p = 2/3$ are more favored by Planck data [11]. Here, in this work, we consider $p = 2/3$ [47, 48] and $p = 4/3$ [47]. The forms of these potentials are shown in Fig. 5. Similarly in the Starobinsky case, inflation occurs from right to left, and the field ϕ slows down near its maximum until it reaches its minimum.

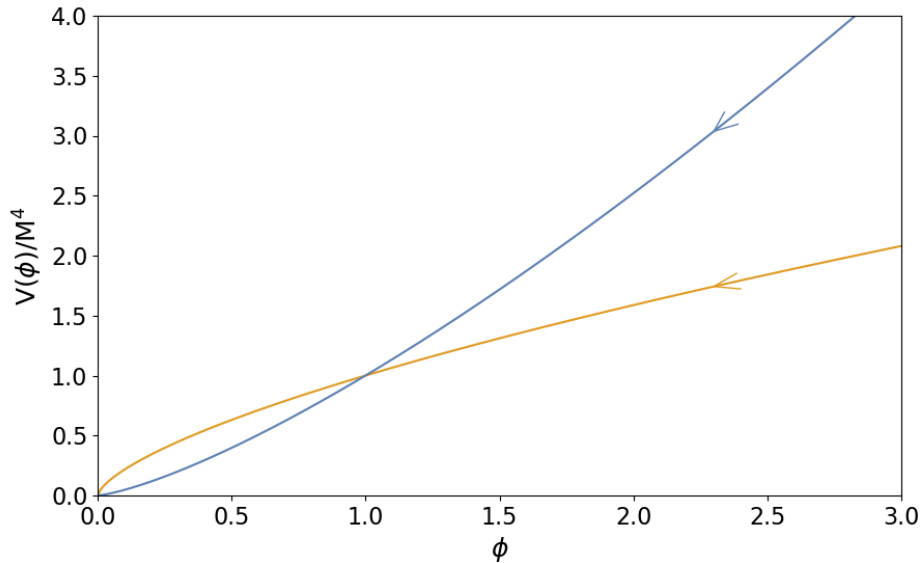


Figure 5: Potential $V(\phi)/M^4$ versus ϕ for large field inflationary models. The orange line corresponds to $p = 2/3$, and the blue line to $p = 4/3$.

The slow-roll parameters are computed from Eqs. (15) and (16), which are given by,

$$\epsilon = \frac{1}{2} \frac{p^2}{\phi^2}, \quad (73)$$

$$\eta = \frac{p(p-1)}{\phi^2}. \quad (74)$$

Recall that inflation ends when $\epsilon = 1$, so we obtain the final value of the scalar field ϕ_{end} ,

$$\phi_{\text{end}} = \frac{p}{\sqrt{2}}. \quad (75)$$

Then, the number of e-foldings is given by,

$$N = \frac{1}{2p} (\phi_{\text{ini}}^2 - \phi_{\text{end}}^2). \quad (76)$$

We set the value of $N \sim 50 - 60$ e-folds, then we obtain the initial value for the scalar field ϕ_{ini} , having,

$$\phi_{\text{ini}} = \sqrt{2pN + \frac{p^2}{2}}. \quad (77)$$

Solving the slow-roll equations allow us to find $a_{\text{sr}}(t)$ and $\phi_{\text{sr}}(t)$, that is,

$$a_{\text{sr}}(t) = \text{Exp} \left\{ \frac{1}{2p} \left\{ \left(\phi_{\text{ini}}^{2-p/2} \right)^{4/(4-p)} - \left[\phi_{\text{ini}}^{2-p/2} + \frac{M^2 p(p-4)}{2\sqrt{3}} t \right] \right\}^{4/(4-p)} \right\}, \quad (78)$$

$$\phi_{\text{sr}}(t) = \left[\phi_{\text{ini}}^{2-p/2} + \frac{M^2 p(p-4)}{2\sqrt{3}} t \right]^{4/(4-p)}, \quad (79)$$

where the parameter M is calculated from Eq. (23) and is given by,

$$M^4 = \frac{12\delta_R p^2 \pi^2}{\phi_*^{p+2}}, \quad (80)$$

where ϕ_* is calculated at the horizon crossing $k = 0.05 \text{ Mpc}^{-1}$.

To solved the equation of motion numerically we integrated Eqs. (1) and (2), using as initial condition the numerical derivative of ϕ_{sr} evaluated at $t = 0$, which is calculated from Eq. (79). The integration was done since $t_{\text{ini}} = 0$ until t_{end} considering $p = 2/3$, and $p = 4/3$. The initial condition for $\phi_{\text{sr}}(0)$ is in each case given by,

$$\dot{\phi}_{\text{sr}}(0) = -\frac{2M^2}{3\sqrt{3}\phi_{\text{ini}}^{2/3}}, \quad \text{for } p = 2/3, \quad (81)$$

$$\dot{\phi}_{\text{sr}}(0) = -\frac{4M^2}{3\sqrt{3}\phi_{\text{ini}}^{1/3}}, \quad \text{for } p = 4/3. \quad (82)$$

Table 4 shows the value of t_{end} for each value of p that we use in our contour plots for the large field inflationary model for $N = 50$, and $N = 60$.

N	p	$t_{\text{end}} \times 10^6 [\text{M}_{\text{Pl}}^{-1}]$
50	$2/3$	2.31907
	$4/3$	1.96204
60	$2/3$	3.09884
	$4/3$	2.77418

Table 4: Value of the time at the end of inflation t_{end} for each value of p in the large field inflationary model.

The scalar power spectrum $P_S(k)$, the scalar spectral index $n_S(k)$, and the tensor-to-scalar ratio r are given by,

$$P_S(k) = \frac{M^4}{144\pi^2 p^2} [(4 - 12C - 5p)p + 12\phi_*^2] \phi_*^p, \quad (83)$$

$$n_S(k) = 1 - \frac{(2+p)p}{\phi_*^2}, \quad (84)$$

$$r = \frac{8p^2}{\phi_*^2}, \quad (85)$$

where ϕ_* is calculated at the horizon crossing $k_* = 0.05 \text{ Mpc}^{-1}$.

6. Discussions and Results

In this section, we present the results using the slow-roll approximation, and those whose coming from our numerical implementation. On the one hand, we calculate the values of A_S and n_S at the pivot scale $k_* = 0.05 \text{ Mpc}^{-1}$ to draw the contour plots (A_S, n_S) . On the other hand, the values of r and n_S are taken at the pivot scale $k_* = 0.002 \text{ Mpc}^{-1}$, yielding the contour plots (r, n_S) . Both calculations utilize the slow-roll approximation to establish the initial conditions. Specifically, to compute A_S , n_S , and r numerically, we fit the values of $P_S(k)$ and $P_T(k)$, given by the expressions (31) and (32). Once these numbers are obtained, we then use them to calculate $n_S(k)$ and r , via Eqs. (9) and (11). It's important to note that the scalar amplitudes do not exactly match the amplitude set at the beginning with the normalization of M . The fitting process adjusts the power-law formula for the scalar spectrum

to ensure an analysis that is not biased by the selection of a specific potential. As a result, while the scalar amplitude will not remain the same, it remains close to the initial COBE normalization value of 2.1×10^{-9} , typically falling within a range from 2.1×10^{-9} to 2.214×10^{-9} [11].

Also, note that in all cases the upshots of r and n_S calculated from our approach are lower than the prediction given by the slow-roll approximation. On the contrary, the numerical values of A_S are larger than those of the slow-roll implementation. This considering the relation between scalar perturbation amplitude and tensor-scalar ratio, if it is obtained that A_S become greater in the numerical approach than in slow roll, this would affect r by definition.

In the following subsections we present the data tables and the contour plots for each model of inflation discussed in section 5. In this point it is important to say that the slow-roll approximation exhibits an error between 0.5 – 1% respect to the numerical results [49, 50].

6.1. Natural Inflation

This model is largely characterized by the Pseudo-Nambu-Goldstone-Boson (PNGB) decay constant f [18, 51]. Hence, different values of the observables are computed by varying this parameter. In Table 5 we show the values of A_S and n_S calculated by changing f , with a pivot scale $k_* = 0.05 \text{ Mpc}^{-1}$. Then, in Table 6 we show the values of r and n_S , again taking several values of f but this time the pivot scale is $k = 0.002 \text{ Mpc}^{-1}$. We present two groups: $N = 50$ and $N = 60$. Note that for larger values of the PNGB constant f , the outcomes reach the ones of the Minimal Chaotic Inflation Model ($V \propto \phi^2$) [52].

In Fig. 6 we present the contour plots (A_S, n_S) and (n_S, r) of the Natural inflation model calculated using the slow-roll approximation with $f = 4, 5, 6, 7, 9, 12, 20, 100$. The left-hand side panel (Fig. 6a) shows the $10^9 A_S$ vs n_S evaluated at $k = 0.05 \text{ Mpc}^{-1}$. And the right-hand side plot (Fig. 6b) is the r vs n_S evaluated at $k = 0.002 \text{ Mpc}^{-1}$. On the other hand, Fig. 7 shows the contour plots aforementioned (A_S, n_S) and (n_S, r) , but these results are now obtained utilizing our numerical approach. In all plots, the black lines represent the results with $N = 60$, while the green ones describe those corresponding to $N = 50$.

Both slow-roll and numerical solutions exhibit a rather small range of improvement with respect to the observational data. In fact, the only outcome that still lies within this window is the case of $N = 60$, where, for instance,

N	f	$\ln(10^{10}A_S)$		n_S	
		SRA	NR	SRA	NR
50	4	3.07185	3.10178	0.928155	0.927331
	5	3.06326	3.08330	0.942521	0.941449
	6	3.05816	3.07471	0.948208	0.946948
	7	3.05499	3.06894	0.950763	0.949435
	9	3.05145	3.06290	0.952733	0.951429
	12	3.04905	3.05899	0.953547	0.952135
	20	3.04707	3.05706	0.953903	0.952306
	100	3.04603	3.05563	0.953976	0.952569
60	4	3.0719	3.09701	0.9325654	0.931436
	5	3.06336	3.07810	0.948956	0.947506
	6	3.05822	3.06930	0.955648	0.954514
	7	3.05501	3.06497	0.958693	0.957331
	9	3.05140	3.05935	0.961051	0.959796
	12	3.04900	3.05535	0.96202	0.960527
	20	3.04701	3.05339	0.962435	0.961124
	100	3.04584	3.05129	0.962514	0.961283

Table 5: Natural inflation values of the amplitude of the scalar power spectrum (A_S) and scalar spectral index (n_S) at the pivot scale $k = 0.05 \text{ Mpc}^{-1}$ changing the parameter f . Both observables are computed utilizing our numerical implementation (NR) and the slow-roll approximation (SRA). We present two sets, one with $N = 50$, and another one with $N = 60$.

the black curve (in Figs. 6a and 7a) slightly reaches the area of 68% C.L.; and on the other hand, this same set plotted in Figs. 6b and 7b travels across only on the 95% C.L..

Finally, note that this model is relevant only for axion decay constants that exceed the Planck scale. This presents a significant theoretical challenge, since quantum gravity effects are anticipated to disrupt the shift symmetry, as well as any global symmetry, at the Planck scale. However, this is not always the case if the symmetry originates from gauge symmetry, as is possible in string theory. Nonetheless, string theory constructions typically result in a decay constant that is below the Planck scale.

N	f	r		n_S	
		SRA	NR	SRA	NR
50	4	0.0301433	0.028223	0.929964	0.929189
	5	0.059850	0.0571789	0.945037	0.944014
	6	0.084651	0.0816419	0.951059	0.950258
	7	0.103267	0.100273	0.953775	0.952636
	9	0.127134	0.124041	0.955871	0.954685
	12	0.145286	0.142484	0.956734	0.955274
	20	0.161567	0.158555	0.957108	0.955798
	100	0.170869	0.168063	0.957183	0.956472
60	4	0.0160243	0.0150583	0.933494	0.932174
	5	0.0381866	0.0366104	0.950453	0.948427
	6	0.059092	0.057291	0.957449	0.956094
	7	0.0757757	0.073799	0.960648	0.959472
	9	0.098969	0.0961345	0.963130	0.962133
	12	0.115622	0.113700	0.964150	0.963000
	20	0.131661	0.129901	0.964585	0.964108
	100	0.140941	0.139356	0.964665	0.964208

Table 6: Natural inflation values of the tensor-to-scalar ratio (r) and scalar spectral index (n_S) at the pivot scale $k = 0.002 \text{ Mpc}^{-1}$ changing the parameter f . Both observables are computed utilizing our numerical implementation (NR) and the slow-roll approximation (SRA). We present two sets, one with $N = 50$, and another one with $N = 60$.

6.2. Hilltop quartic inflation

In this subsection we present the Hilltop quartic inflation results varying the parameter μ . In Table 7 we show the values of A_S and n_S , with a pivot scale $k_* = 0.05 \text{ Mpc}^{-1}$. Then, in Table 8 we show the values of r and n_S but this time the pivot scale is $k = 0.002 \text{ Mpc}^{-1}$. We display two groups: $N = 50$, and $N = 60$.

Furthermore, Fig. 8 shows the contour plots (A_S, n_S) and (n_S, r) of the Hilltop quartic inflationary model calculated using the slow-roll approximation with $\mu = 7, 9, 11, 13, 15, 18, 25, 35, 95$. The left-hand side panel (Fig. 8a) shows the $10^9 A_S$ vs n_S evaluated at $k = 0.05 \text{ Mpc}^{-1}$. And the right-hand side plot (Fig. 8b) is the r vs n_S evaluated at $k = 0.002 \text{ Mpc}^{-1}$. On the other hand, in Fig. 9 we present the contour plots aforementioned (A_S, n_S) and

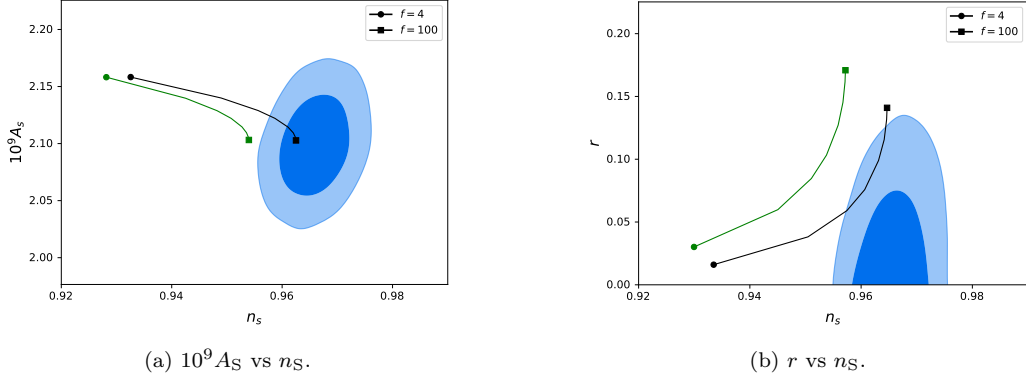


Figure 6: Contour plots (A_S, n_S) and (n_S, r) of the Natural inflation model calculated using the slow-roll approximation with $f = 4, 5, 6, 7, 9, 12, 20, 100$, where the black lines represent results with $N = 60$, while the green ones describe those corresponding to $N = 50$. The panel on the left-hand side (a) shows the $10^9 A_S$ vs n_S evaluated at $k = 0.05 \text{ Mpc}^{-1}$. And the right-hand side plot (b) is the r vs n_S evaluated at $k = 0.002 \text{ Mpc}^{-1}$.

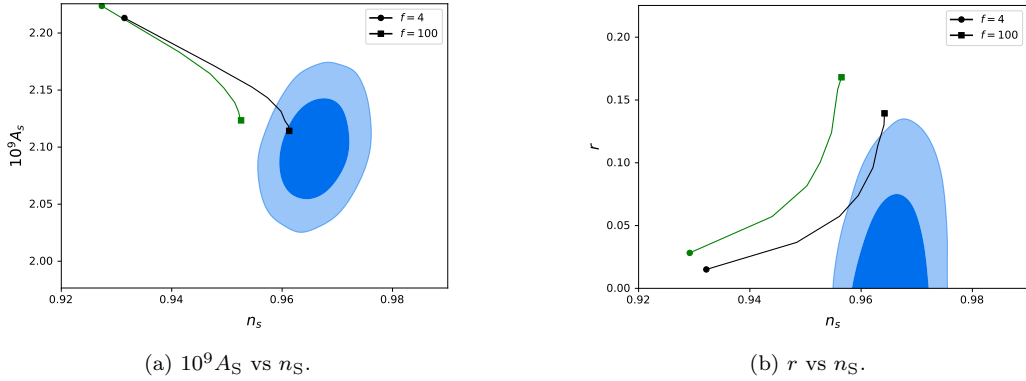


Figure 7: Contour plots (A_S, n_S) and (n_S, r) of the Natural inflation model calculated using our numerical implementation with $f = 4, 5, 6, 7, 9, 12, 20, 100$, where the black lines represent results with $N = 60$, while the green ones describe those corresponding to $N = 50$. The panel on the left-hand side (a) shows $10^9 A_S$ vs n_S evaluated at $k = 0.05 \text{ Mpc}^{-1}$. And the plot on the right-hand side (b) is the r vs n_S evaluated at $k = 0.002 \text{ Mpc}^{-1}$.

(n_S, r) but now these results are obtained utilizing our numerical approach. In all plots, the black lines represent the results with $N = 60$, while the green ones describe those corresponding to $N = 50$. Note that in both sets of results there is an important range of parameter μ that are well inside the observational area. Therefore, this potential is highly favored by the Planck 2018 data [11].

N	μ	$\ln(10^{10}A_S)$		n_S	
		SRA	NR	SRA	NR
50	7	3.07052	3.09027	0.940847	0.940734
	9	3.06843	3.08463	0.945673	0.945371
	11	3.06654	3.08195	0.949481	0.949044
	13	3.06489	3.07888	0.952421	0.951854
	15	3.06350	3.07612	0.954682	0.954083
	18	3.06181	3.07163	0.957151	0.956450
	25	3.05903	3.06787	0.960424	0.959750
	35	3.05685	3.06545	0.962470	0.961947
	95	3.05321	3.05801	0.964594	0.963570
60	7	3.06681	3.07965	0.950729	0.950145
	9	3.06519	3.07708	0.954468	0.953959
	11	3.06365	3.07457	0.957556	0.956850
	13	3.06229	3.07004	0.96003	0.959112
	15	3.06109	3.06864	0.961988	0.961235
	18	3.05960	3.06521	0.964187	0.963125
	25	3.05724	3.06218	0.967196	0.966246
	35	3.05525	3.0575	0.969133	0.968019
	95	3.05192	3.05241	0.971179	0.969734

Table 7: Hilltop quartic inflation values of the amplitude of the scalar power spectrum (A_S) and scalar spectral index (n_S) at the pivot scale $k = 0.05 \text{ Mpc}^{-1}$ changing the parameter μ . Both observables are computed utilizing our numerical implementation (NR) and the slow-roll approximation (SRA). We present two sets, one with $N = 50$ and another one with $N = 60$.

6.3. Starobinsky inflationary model

The Starobinsky scenario is remarkably simple, hence only two instance are shown: one for $N = 50$ and another one for $N = 60$. In Table 9 we show the values of A_S and n_S with a pivot scale $k_* = 0.05 \text{ Mpc}^{-1}$. Then, in Table 10 we show the values of r and n_S but this time the pivot scale is $k = 0.002 \text{ Mpc}^{-1}$.

Furthermore, Fig. 10 shows the contour plots (A_S, n_S) and (n_S, r) of the Starobinsky inflationary model calculated using the slow-roll approximation. The left-hand side panel (Fig. 10a) shows $10^9 A_S$ vs n_S evaluated

N	μ	r		n_s	
		SRA	NR	SRA	NR
50	7	0.00348786	0.00331328	0.944542	0.944323
	9	0.00675914	0.00645695	0.948953	0.948583
	11	0.0106721	0.0102239	0.952493	0.952214
	13	0.0148423	0.0142607	0.955261	0.954877
	15	0.0189986	0.0183029	0.957412	0.956919
	18	0.0248786	0.0241033	0.959785	0.959142
	25	0.0362140	0.0352731	0.962960	0.963110
	35	0.0473473	0.0462421	0.964966	0.964971
	95	0.0703695	0.0691776	0.967064	0.966904
60	7	0.00213601	0.00204658	0.953265	0.952087
	9	0.00430359	0.0041428	0.956743	0.955900
	11	0.00703314	0.0067919	0.959637	0.959287
	13	0.0100659	0.00975431	0.961980	0.961175
	15	0.0131925	0.0128254	0.963851	0.963906
	18	0.0177647	0.0173165	0.965969	0.965293
	25	0.0269608	0.0263789	0.968899	0.968298
	35	0.0363702	0.0357350	0.970804	0.969874
	95	0.0566272	0.0558734	0.972827	0.971642

Table 8: Hilltop quartic inflation values of the tensor-to-scalar ratio (r) and scalar spectral index (n_s) at the pivot scale $k = 0.002 \text{ Mpc}^{-1}$ changing the parameter μ . Both observables are computed utilizing our numerical implementation (NR) and the slow-roll approximation (SRA). We present two sets, one with $N = 50$, and another one with $N = 60$.

at $k = 0.05 \text{ Mpc}^{-1}$. And the right-hand side plot (Fig.10b) is the r vs n_s evaluated at $k = 0.002 \text{ Mpc}^{-1}$. On the other hand, in Fig. 9 we present the aforementioned contour plots (A_s, n_s) and (n_s, r) but now these results are obtained utilizing our numerical approach. In all plots, the black dots represent the results with $N = 60$, while the green ones describe those corresponding to $N = 50$.

The numerical and slow-roll upshots are very similar; however, the numerical r is visibly lower than the slow-roll one. Additionally, this time only the black points ($N = 60$) are well within the area of both observables.

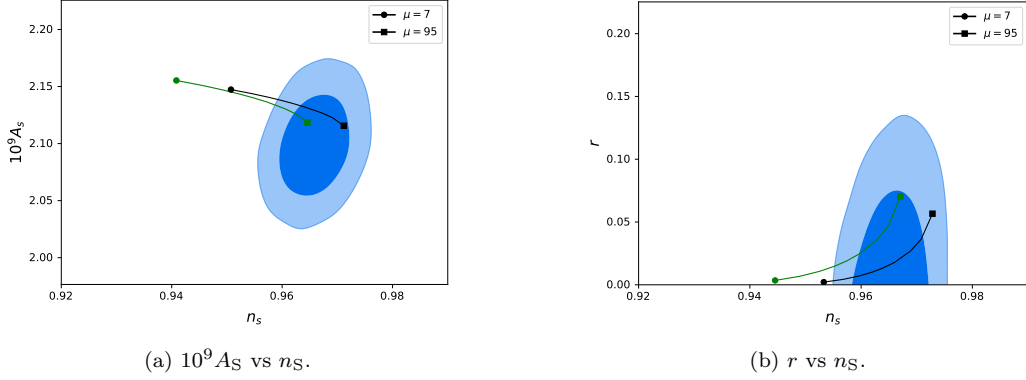


Figure 8: Contour plots (A_S, n_S) and (n_S, r) of the Hilltop quartic inflation model calculated using the slow-roll approximation with $\mu = 7, 9, 11, 13, 15, 18, 25, 35, 95$, where the black lines represent results with $N = 60$, while the green ones describe those corresponding to $N = 50$. The left-hand side panel (a) shows $10^9 A_S$ vs n_S evaluated at $k = 0.05 \text{ Mpc}^{-1}$. And the plot on the right-hand side (b) is the r vs n_S evaluated at $k = 0.002 \text{ Mpc}^{-1}$.

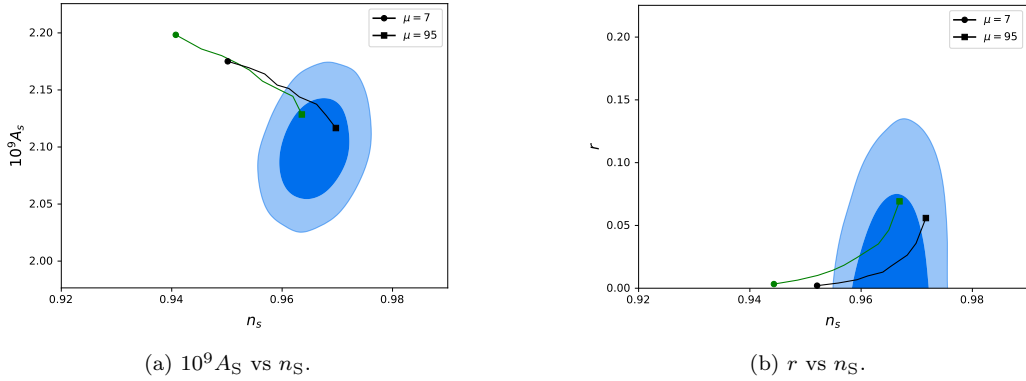


Figure 9: Contour plots (A_S, n_S) and (n_S, r) of the Hilltop quartic inflation model calculated using our numerical implementation with $\mu = 7, 9, 11, 13, 15, 18, 25, 35, 95$, where the black lines represent results with $N = 60$, while the green ones describe those corresponding to $N = 50$. The left-hand side panel (a) shows $10^9 A_S$ vs n_S evaluated at $k = 0.05 \text{ Mpc}^{-1}$. And the plot on the right-hand side (b) is the r vs n_S evaluated at $k = 0.002 \text{ Mpc}^{-1}$.

6.4. Large field inflation models

The Large field inflationary models are also a simple scenario due to its unique parameter p . Hence, we present only two results with $p = 2/3$ and $p = 4/3$. In Table 11 we show the values of A_S and n_S with a pivot scale

N	$\ln(10^{10}A_S)$		n_S	
	SRA	NR	SRA	NR
50	3.06550	3.07514	0.953663	0.953222
60	3.06204	3.06776	0.962336	0.961705

Table 9: Starobinsky inflation values of the amplitude of the scalar power spectrum (A_S) and scalar spectral index (n_S) at the pivot scale $k = 0.05 \text{ Mpc}^{-1}$. Both observables are computed utilizing our numerical implementation (NR) and the slow-roll approximation (SRA). We present two sets, one with $N = 50$, and another one with $N = 60$.

N	r		n_S	
	SRA	NR	SRA	NR
50	0.00523324	0.00504663	0.956926	0.955919
60	0.00403100	0.00349071	0.964515	0.963774

Table 10: Starobinsky inflation values of the tensor-to-scalar ratio (r) and scalar spectral index (n_S) at the pivot scale $k = 0.002 \text{ Mpc}^{-1}$. Both observables are computed utilizing our numerical implementation (NR) and the slow-roll approximation (SRA). We present two sets, one with $N = 50$ and another one with $N = 60$.

$k_* = 0.05 \text{ Mpc}^{-1}$. Then, in Table 12 we show the values of r and n_S but this time the pivot scale is $k = 0.002 \text{ Mpc}^{-1}$.

Furthermore, Fig. 12 shows the contour plots (A_S, n_S) and (n_S, r) of the Large field power-law potentials model calculated using the slow-roll approximation. The left panels (Figs. 12a and 12c) show the $10^9 A_S$ vs n_S evaluated at $k = 0.05 \text{ Mpc}^{-1}$. And the right plots (Figs. 12b and 12d) is the r vs n_S evaluated at $k = 0.002 \text{ Mpc}^{-1}$. On the other hand, in Fig. 13 we present the aforementioned contour plots (A_S, n_S) and (n_S, r) but now these results are obtained utilizing our numerical approach. In all plots, the black dots represent the results with $N = 60$, while the green ones describe those corresponding to $N = 50$.

The analysis of two distinct cases is as follows. For $p = 2/3$ at $N = 50$ both the numerical and slow-roll outcomes lie within the observation window (at 68% C.L.). In contrast, at $N = 60$ only the numerical upshot is contained at the 95% C.L.; hence our method improves this prediction. On the other

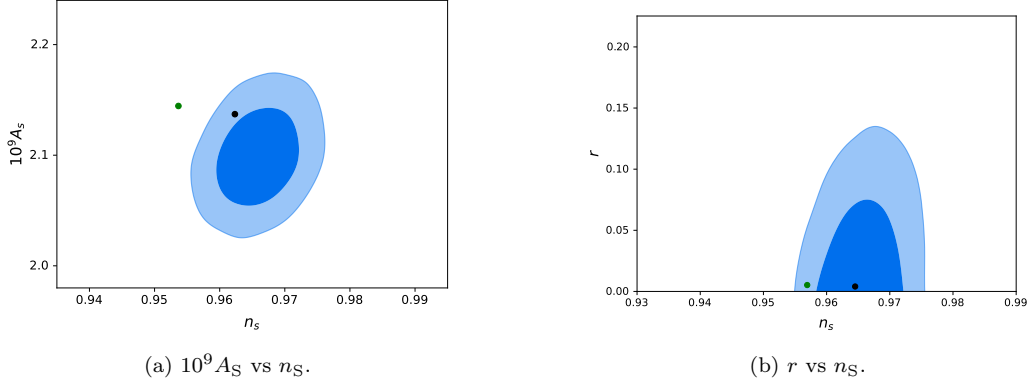


Figure 10: Contour plots (A_S, n_S) and (n_S, r) of the Starobinsky inflationary model calculated using the slow-roll approximation, where the black dots represent the results with $N = 60$, while the green ones describe those corresponding to $N = 50$. The left-hand side panel (a) shows $10^9 A_S$ vs n_S evaluated at $k = 0.05 \text{ Mpc}^{-1}$. And the plot on the right-hand side (b) is the r vs n_S evaluated at $k = 0.002 \text{ Mpc}^{-1}$.

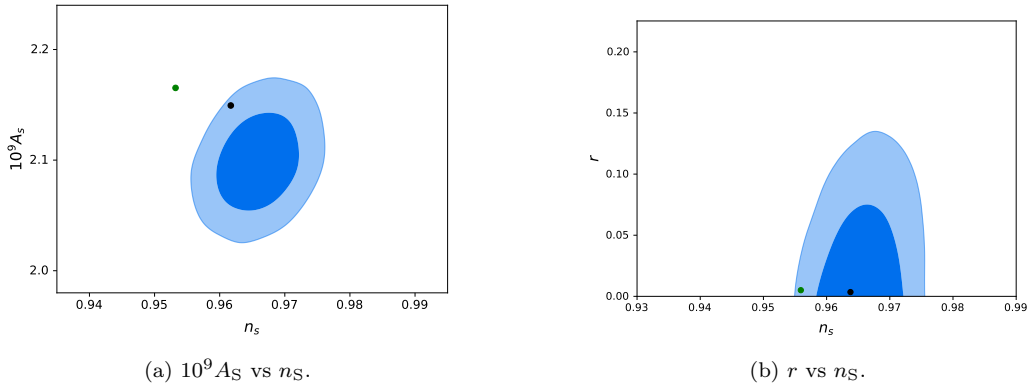


Figure 11: Contour plots (A_S, n_S) and (n_S, r) of the Starobinsky inflationary model calculated using our numerical implementation, where the black dots represent the results with $N = 60$, while the green ones describe those corresponding to $N = 50$. The left-hand side panel (a) shows $10^9 A_S$ vs n_S evaluated at $k = 0.05 \text{ Mpc}^{-1}$. And the plot on the right-hand side (b) is the r vs n_S evaluated at $k = 0.002 \text{ Mpc}^{-1}$.

hand, for example, $p = 4/3$ all points sit inside 95% C.L. or 68% C.L., and the single contrast emerges at $N = 50$ since the numerical solution shifts the point from the 1σ 's to the 2σ 's zones.

N	p	$\ln(10^{10}A_S)$		n_S	
		SRA	NR	SRA	NR
50	$2/3$	3.05286	3.05574	0.968689	0.967558
	$4/3$	3.04937	3.05718	0.961322	0.960497
60	$2/3$	3.05141	3.05172	0.974593	0.973154
	$4/3$	3.04861	3.05272	0.968546	0.967468

Table 11: Large field power-law potentials inflation values of the amplitude of the scalar power spectrum (A_S) and scalar spectral index (n_S) at the pivot scale $k = 0.05 \text{ Mpc}^{-1}$ with $p = 2/3, 4/3$. Both observables are computed utilizing our numerical implementation (NR) and the slow-roll approximation (SRA). We present two sets, one with $N = 50$ and another one with $N = 60$.

N	p	r		n_S	
		SRA	NR	SRA	NR
50	$2/3$	0.0582048	0.0572722	0.970898	0.969751
	$4/3$	0.115105	0.113198	0.96403	0.963526
60	$2/3$	0.0478681	0.0472768	0.976066	0.974887
	$4/3$	0.0948539	0.0936424	0.970358	0.969395

Table 12: Large field power-law potentials inflation values of the tensor-to-scalar ratio (r) and scalar spectral index (n_S) at the pivot scale $k = 0.002 \text{ Mpc}^{-1}$ with $p = 2/3, 4/3$. Both observables are computed utilizing our numerical implementation (NR) and the slow-roll approximation (SRA). We present two sets, one with $N = 50$, and another one with $N = 60$.

Acknowledgements

One of the authors, C. Rojas, wants to thank Gabriel Germán, and Jessica Cook for useful discussions. R.H.J. is supported by CONAHCYT Estancias Posdoctorales por México, Modalidad 1: Estancia Posdoctoral Académica and by SNI-CONAHCYT.

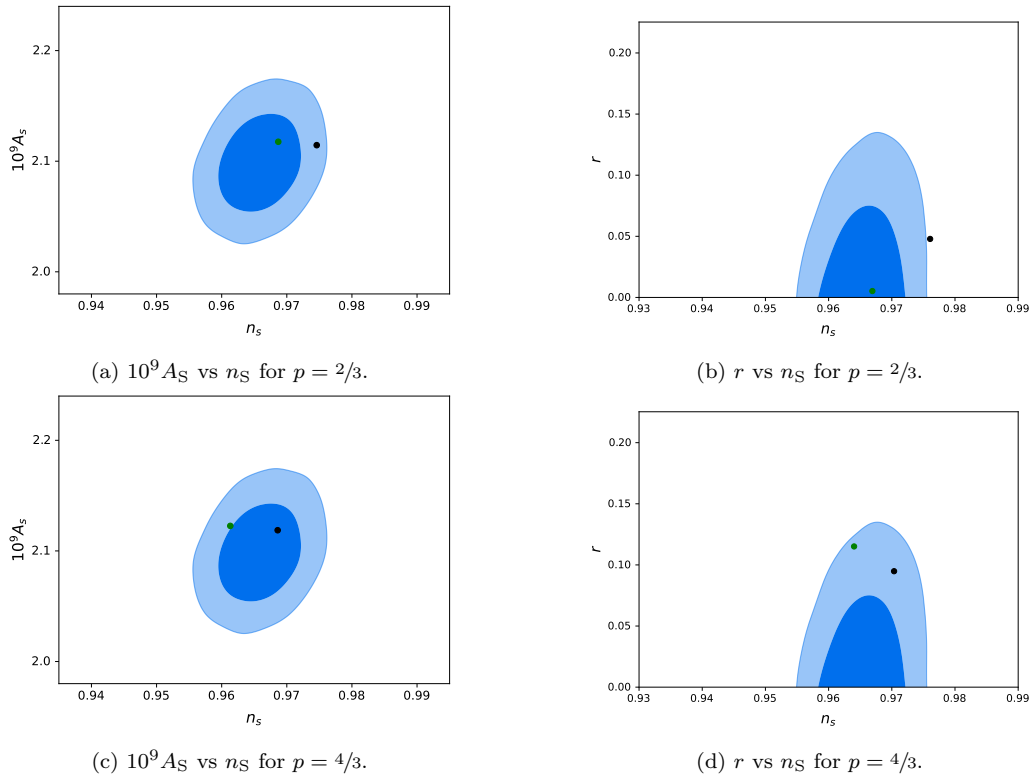


Figure 12: Contour plots (A_S, n_S) and (n_S, r) of the Large field power-law potentials model calculated using the slow-roll approximation, where the black dots represent the results with $N = 60$, while the green ones describe those corresponding to $N = 50$. The left panels show the $10^9 A_S$ vs n_S evaluated at $k = 0.05 \text{ Mpc}^{-1}$: (a) with $p = 2/3$ and (c) $p = 4/3$. And the right plots are the r vs n_S evaluated at $k = 0.002 \text{ Mpc}^{-1}$: (b) with $p = 2/3$, and (d) $p = 4/3$.

7. Conclusions

In this study, we investigated four widely recognized inflationary scenarios, as presented by the most recent Planck observations: Natural inflation, Hilltop quartic inflation, the Starobinsky inflationary model, and Large field power-law potentials, denoted by $V(\phi) \sim \phi^p$, where we considered specific values such as $p = 2/3$ and $4/3$.

Our analysis mainly consisted of a comparison between the slow-roll approximation and our numerical implementation; where the latter yields better results. On the one hand, we calculate the values of A_S and n_S at the pivot scale $k_* = 0.05 \text{ Mpc}^{-1}$ to draw the contour plots (A_S, n_S) . On the other

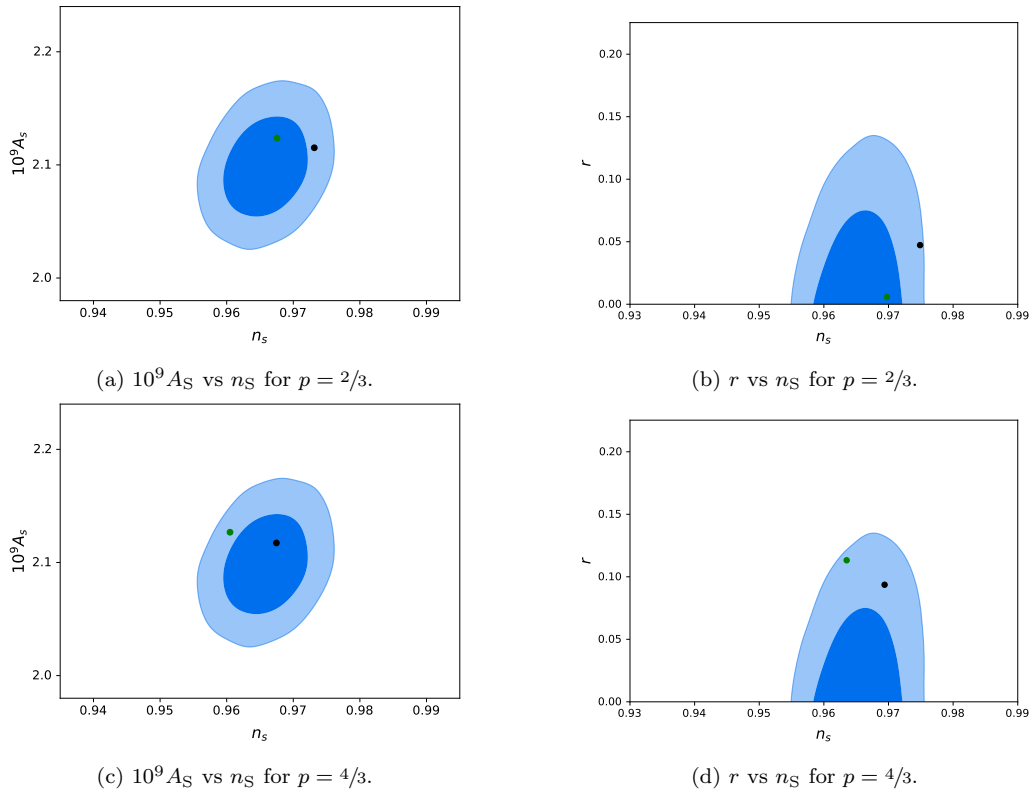


Figure 13: Contour plots (A_S, n_S) and (n_S, r) of the Large field power-law potentials model calculated using our numerical implementation, where the black dots represent the results with $N = 60$, while the green ones describe those corresponding to $N = 50$. The left panels show the $10^9 A_S$ vs n_S evaluated at $k = 0.05 \text{ Mpc}^{-1}$: (a) with $p = 2/3$ and (c) $p = 4/3$. And the right plots are the r versus n_S evaluated in $k = 0.002 \text{ Mpc}^{-1}$: (b) with $p = 2/3$, and (d) $p = 4/3$.

hand, the values of r and n_S are taken at the pivot scale $k_* = 0.002 \text{ Mpc}^{-1}$, yielding the contours plots (r, n_S) . Both calculations utilize the slow-roll approximation to set the initial conditions.

In Natural inflation, both slow-roll and numerical solutions demonstrated a relatively limited degree of enhancement concerning the observational data. In fact, the only outcome that remained consistent within this range was the case of $N = 60$.

The Hilltop quartic inflation model is characterized by η , and in both sets of results, there is an important range of this parameter that is well inside the observational area. Thus, this potential is strongly supported by

the Planck 2018 data [11].

Although the Starobinsky scenario is remarkably simple, the case of $N = 60$ is well within the area of all observables. Moreover, both the numerical and slow-roll upshots are very similar; however, the numerical r is visibly lower than the slow-roll estimation.

Finally, the Large field power-law potentials analysis of two distinct cases resulted as follows. In the scenario where $p = 2/3$ at $N = 50$, both the numerical and slow-roll outcomes remained within the observation window (at 68% C.L.). However, when considering $N = 60$, only the numerical upshot fell within the 95% C.L., highlighting an enhancement in our method's predictive capability. In contrast, in the case of $p = 4/3$, all data points were placed within the 95% C.L. or 68% C.L., except for a single deviation occurring at $N = 50$ where the numerical solution shifted the point from the 1σ to the 2σ zones.

In general, our study demonstrated that the numerical solution improved the precision of these models with respect to the contour plot r vs. n_s . This was evidenced by consistently lower values of r in each model compared to the values derived from the slow-roll approximation.

In conclusion, we expect this thoroughly task to provide a well-described route on the study of inflationary physics and its corresponding observational signature and its contrast with the available most current relevant data.

References

- [1] A. Albrecht and P. J. Steinhardt. Cosmology for Grand Unified Theories with Radiatively Induced Symmetry Breaking. *Phys. Rev. Lett.*, 48:1220, 1982.
- [2] A. H. Guth. Inflationary universe: A possible solution to the horizon and flatness problems. *Phys. Rev. D*, 23:347, 1981.
- [3] A. D. Linde. A New Inflationary Universe Scenario: A Possible Solution of the Horizon, Flatness, Homogeneity, Isotropy and Primordial Monopole Problems. *Phys. Lett. B*, 108:389, 1982.
- [4] A. A. Starobinsky. A New Type of Isotropic Cosmological Models Without Singularity. *Phys. Lett. B*, 91:99, 1980.
- [5] K. Sato. First Order Phase Transition of a Vacuum and Expansion of the Universe. *Mon. Not. Roy. Astron. Soc.*, 195:467, 1981.

- [6] S. Weinberg. *Cosmology*. OUP Oxford, 2008.
- [7] J. A. Vazquez, L. E. Padilla, and T. Matos. Inflationary cosmology: from theory to observations. *Rev. Mex. Fis. E*, 17:73, 2020.
- [8] J. Preskill. Cosmological Production of Superheavy Magnetic Monopoles. *Phys. Rev. Lett.*, 43:1365, 1979.
- [9] S. D. Odintsov, V. K. Oikonomou, I. Giannakoudi, F. P. Fronimos, and E. C. Lympriadou. Recent Advances on Inflation. *Symmetry*, 15:1701, 2023.
- [10] J. Martin. Inflationary perturbations: The cosmological Schwinger effect. *Lecture Notes in Physics*, 738:193, 2008.
- [11] Y. Akrami *et al.* Planck 2018 results. X. Constraints on inflation. *Astron. Astrophys.*, 641:A10, 2020.
- [12] S. Habib and A. Heinen and K. Heitmann and G. Jungman. Inflationary Perturbations and Precision Cosmology. *Phys. Rev. D*, 71:043518, 2005.
- [13] W. Giarè, M. De Angelis, C. van de Bruck, and E. Di Valentino . Tracking the Multifield Dynamics with Cosmological Data: A Monte Carlo approach. *JCAP*, 12:014, 2023.
- [14] G. Germán, J. C. Hidalgo, and L. E. Padilla. Inflationary models constrained by reheating. *arXiv:1404.6704*, 2023.
- [15] J. Martin, C. Ringeval, and V. Vennin. Encyclopaedia Inflationaris. *Phys. Dark Univ.*, 5–6:75, 2014.
- [16] J. Martin, and C. Ringeval. Inflation after WMAP3: confronting the slow-roll and exact power spectra with CMB data. *JCAP*, 24:009, 2006.
- [17] K. Freese, J. A. Frieman, and A. V. Olinto. Natural inflation with pseudo Nambu–Goldstone bosons. *Phys. Rev. Lett.*, 65:3233, 1990.
- [18] F. C. Adams, J. R. Bond, K. Freese, J. A. Fireman, and A. V. Olinto. Natural inflation: Particle physics models, power-law spectra for large-scale structure, and constraints from the Cosmic Background Explorer. *Phys. Rev. D*, 47:426, 1993.

- [19] L. Boubekeur and D. H. Lyth. Hilltop inflation. *JCAP*, 07:010, 2005.
- [20] A. A. Starobinsky. A new type of isotropic cosmological models without singularity. *Phys. Lett. B*, 91:99, 1980.
- [21] A. D. Linde. Chaotic Inflation. *Phys. Rev. D*, 129B:177, 1983.
- [22] A. R. Liddle and D. H. Lyth. *Cosmological inflation and large-scale structure*. Cambridge University Press, 2000.
- [23] E. J. Copeland, E. W. Kolb, A. R. Liddle, and J. E. Lidsey. Observing the Inflaton Potential. *Phys. Rev. Letts*, 71, 1993.
- [24] P. Adshead, R. Easther, J. Pritchard, and A. Loeb. Inflation and the scale dependent spectral index: prospects and strategies. *JCAP*, 02:021, 2011.
- [25] H. V. Ragavendra, and L. Sriramkumar. Observational Imprints of Enhanced Scalar Power on Small Scales in Ultra Slow Roll Inflation and Associated Non-Gaussianities . *Galaxies*, 11, 2023.
- [26] W. Giarè, S. Pan, E. Di Valentino, W. Yang, J. de Haro, and A. Melchiorri. Inflationary Potential as seen from Different Angles: Model Compatibility from Multiple CMB Missions. *arXiv:2305.15378v1*, 2023.
- [27] J. A. Vazquez, M. Bridges, Y-Z. Ma, and M. P. Hobson. Constraints on the tensor-to-scalar ratio for non-power-law models. *JCAP*, 08:001, 2013.
- [28] S. Das and R. O. Ramos. Running and Running of the Running of the Scalar Spectral Index in Warm Inflation. *Universe*, 9:76, 2023.
- [29] F. Finelli *et al.* Exploring cosmic origins with CORE: Inflation. *JCAP*, 04:016, 2018.
- [30] K. Freese, and W. H. Kinney. Natural inflation: consistency with cosmic microwave background observations of Planck and BICEP2. *JCAP*, 03:044, 2015.
- [31] N. K. Stein, and W. H. Kinney. Natural inflation after Plack 2018. *JCAP*, 01:022, 2022.

- [32] N. K. Stein, and W. H. Kinney. Natural inflation after Plack 2018. *JCAP*, 01:022, 2022.
- [33] G. Montefalcone, V. Aragam, L. Visinelli, and K. Freese. Observational constraints on warm natural inflation. *JCAP*, 03:002, 2023.
- [34] J. L. Cook. Primordial Black Hole Production in Natural and Hilltop Inflation. *JCAP*, 07:031, 2023.
- [35] G. Germán. Quartic hilltop inflation revisited. *JCAP*, 02:034, 2021.
- [36] N. K. Stein, and W. H. Kinney. Simple single-field inflation models with arbitrarily small tensor/scalar ratio. *JCAP*, 03:027, 2022.
- [37] J. Hoffmann and D. Sloan. Regularization of Single Field Inflation Models. *Phys. Rev. D*, 2023.
- [38] H. G. Lillepalu and A. Racioppi. Generalized Hilltop Inflation. *EPJ Plus*, 138:894, 2023.
- [39] R. Kallosh and A. Linde. An analytic treatment of quartic hilltop inflation. *Phys. Lett. B*, 809:135688, 2020.
- [40] R. Kallosh and A. Linde. On hilltop and brane inflation after Planck. *JCAP*, 09:030, 2019.
- [41] S. Antusch, D. Nolde, and S. Orani . Hill crossing during preheating after hilltop inflation. *JCAP*, 06:009, 2015.
- [42] J. C. Bueno Sánchez, M. Bestero-Gil, A. Berera, and K. Dimopoulos. Warm hilltop inflation. *Phys. Rev. D*, 77:123527, 2008.
- [43] C. Rojas. Study of scalar and tensor power spectra in the generalized Starobinsky inflationary model using semiclassical methods. *Astroparticle Physics*, 143:102745, 2022.
- [44] J. Martin. Cosmic Inflation: Trick or Treat? *arXiv:1902.05286*, 2019.
- [45] E. Di Valentino and L. Mersini-Houghton. Testing predictions of the quantum landscape multiverse 1: the Starobinsky inflationary potential. *JCAP*, 2, 2017.

- [46] L. McAllister, E. Silverstein, and A. Westphal. Gravity waves and linear inflation from axion monodromy. *Phys. Rev. D*, 82:046003, 2010.
- [47] L. McAllister, E. Silverstein, A. Westphal, and T. Wrase. The powers of monodromy. *JHEP*, 09:123, 2014.
- [48] E. Silverstein and A. Westphal. Monodromy in the CMB: Gravity waves and string inflation. *Phys. Rev. D*, 78:106003, 2008.
- [49] C. Rojas and V. M. Villalba. Computation of inflationary cosmological perturbations in chaotic inflationary scenarios using the phase-integral method. *Phys. Rev. D*, 79:103502, 2009.
- [50] C. Rojas and V. M. Villalba. Computation of the power spectrum in chaotic $\frac{1}{4}\lambda\phi^4$ inflation. *JCAP*, 003:1, 2012.
- [51] J. E. Kim, H. P. Nilles, and M. Peloso. Completing natural inflation. *JCAP*, 005, 2005.
- [52] M. Escudero, H. Ramírez, L. Boubekeur, E. Giusarma, and O. Mena. The present and future of the most favoured inflationary models after Planck 2015. *JCAP*, 020, 2016.